Food Packaging and Shelf Life 54 (2026) 101728

Contents lists available at ScienceDirect

Food Packaging and Shelf Life

journal homepage: www.elsevier.com/locate/fpsl

# Microfibrillated cellulose films from agri-food wastes and plant residues for food packaging applications – A comparative investigation

Tommaso Bellesia [a], Daniele Carullo [a], Andrea Fachin [a], Maral Soltanzadeh [a], Masoud Ghaani [b], Giorgio Innocenzo Ascrizzi [c], Laura Piazza [c], Stefano Farris [a,*]

[a] Department of Food, Environmental and Nutritional Sciences (DeFENS), Food Packaging Laboratory, University of Milan, Milan, Italy
[b] Department of Civil, Structural & Environmental Engineering, Trinity College Dublin, Dublin, Ireland
[c] Department of Environmental Science and Policy (ESP), University of Milan, Milan, Italy

ARTICLE INFO

*Keywords:*
Biopolymer
Circular economy
High pressure homogenization
Microscopy
Permeability
Wettability

ABSTRACT

Cellulose from three agri-waste feedstocks—giant cane, *Posidonia oceanica* seagrass, and coffee silverskin—was processed into aqueous dispersions (1% by weight) of microfibrillated cellulose (MFC) via high-pressure homogenization (HPH) to produce stand-alone films for potential food packaging applications. Rheology, stability, and morphology of dispersions, as well as optical, barrier, mechanical, morphological, and surface properties of the resulting films were evaluated, with Sylvicta® used as a commercial reference. Atomic Force Microscopy (AFM) confirmed successful MFC production (average diameter $< 100$ nm) after HPH. The dispersions showed good stability ($\zeta$-potential $< 30$ mV), shear-thinning, and strong-gel behavior ($G'/G'' \approx 10$). Regardless of cellulose source, the films performed similarly to the commercial solution, including excellent oxygen barrier properties [oxygen transmission rate $< 0.01$ $cm^3$ (STP) $m^{-2}$ $day^{-1}$ under dry test conditions], high stiffness (Young's modulus $\approx 7.5$ GPa), tensile strength ($\approx 85$ MPa), and effective UV-shielding. Surface wettability differed: the commercial sample exhibited a higher contact angle ($\approx 115°$) than the prepared films ($\approx 55$–$95°$). Nonetheless, all samples showed initial spreading of the water droplet followed by absorption. This study demonstrates the potential of valorizing agri-food waste and plant residues into sustainable, high-performance cellulosic films for food packaging. The approach supports circular economy strategies and helps reduce the environmental impact of plastics.

## 1. Introduction

The unceasing consumer demand for high-quality, safer products, combined with growing awareness of the environmental impact of petroleum-based plastic mismanagement, has prompted the development of more sustainable food packaging materials derived from renewable sources, such as agri-food wastes and plant residues (Orqueda et al., 2022; Urena et al., 2024; Yu et al., 2024). However, these materials can only enter the market if they replicate the functionality of conventional plastics (i.e., mechanical, oxygen and water vapor barrier, optical, and thermal properties) while ensuring shelf-life extension (Ghasemlou et al., 2024; Spence et al., 2010; Thomas et al., 2023).

Recent estimates indicate that about 1.5 billion tons of agricultural wastes and plant residues are generated worldwide each year (Ezeorba et al., 2024; Padhi et al., 2023). At present, these biomasses are mainly used for low value-added purposes (e.g., animal feed and fertilizers) or sent to composting/incineration (Bassani et al., 2022; García et al., 2016), which limits exploitation of their full potential (Aguiló-Aguayo et al., 2024; Espinosa et al., 2022; Mapelli et al., 2022; Sabater et al., 2022). Agri-food wastes and plant residues can be effectively exploited for the extraction of biopolymers—such as cellulose, hemicellulose, and lignin—for the synthesis of biodegradable food packaging materials (Dubey et al., 2023; Rostamabadi et al., 2024). In this context, cellulose has long been the focus of industrial research for several reasons. First, it represents the most abundant fiber fraction in the aforementioned sources ($\approx$ 20–50% by weight of the original biomass), with a content comparable to that of conventional raw materials such as wood and cotton (Rovera et al., 2023). Second, cellulose is biodegradable, biocompatible, non-toxic, and both thermally and mechanically stable (Salas et al., 2014; Wei et al., 2023). Third, when recovered through economically feasible processes with high yield and purity, it can serve multiple industrial sectors (Khan et al., 2022). To date, the extraction of

* Corresponding author.
*E-mail address:* stefano.farris@unimi.it (S. Farris).

https://doi.org/10.1016/j.fpsl.2026.101728
Received 14 September 2025; Received in revised form 24 January 2026; Accepted 2 March 2026
Available online 5 March 2026

cellulose from diverse agri-food wastes and plant residues has been extensively documented in the literature (Araújo et al., 2019; Bellesia et al., 2024; Ramos et al., 2023; Romruen et al., 2022; Sayanjali et al., 2024; Thongsomboon et al., 2023). Nevertheless, inherent drawbacks such as high porosity, low microbial resistance, and poor gas and vapor barrier properties limit the applicability of fully cellulosic materials (e.g., paper and paperboard) mainly to food containment and transport (Jin et al., 2021; Wang et al., 2022). When food protection and shelf-life extension are required, paper and paperboard are often coupled with plastic polymers or aluminum foil through lamination or co-extrusion. This results in multi-layer paper-based packaging with superior barrier and mechanical performance (Rovera et al., 2020). However, the heterogeneous structure of such systems severely hinders end-of-life management due to limited recyclability (Mujtaba et al., 2022; Shorey & Mekonnen, 2022).

More recently, microfibrillated cellulose (MFC) has emerged as a greener alternative to plastics for food packaging applications (Dou et al., 2021; Qi et al., 2020; Zhang et al., 2023). MFC consists of cellulose nanofibers that are nano-wide (up to 100 nm) and micro-long (up to several μm), exhibiting both amorphous and crystalline domains (Luo et al., 2021; Ortiz et al., 2018). The high aspect ratio and the excellent film-forming capacity of MFC make it ideal for producing films with outstanding optical, tensile, and gas barrier properties (Amoroso et al., 2022; Samsalee et al., 2023; Spence et al., 2010). Various top-down approaches have been proposed for producing MFC, including chemical methods (e.g., acid hydrolysis, TEMPO oxidation), mechanical methods (e.g., high-pressure homogenization, ball milling), and enzymatic approaches (Kim et al., 2021; Pirozzi et al., 2021; Wang et al., 2024).

High-pressure homogenization (HPH) is a purely mechanical process in which a solution or dispersion is subjected to high pressures (50–300 MPa) through a micrometric chamber, followed by an abrupt pressure drop as the material exits the unit (Carullo et al., 2018). This generates intense fluid-mechanical stresses—such as cavitation, shear, turbulence, and elongation—occurring rapidly within the system (Coccaro et al., 2018). In particular, treatment of cellulosic pulp with HPH induces cellulose defibrillation, thereby promoting its conversion into MFC (Pirozzi et al., 2023). Overall, due to its high efficiency, industrial scalability, and environmental friendliness, HPH is generally preferred over chemical and enzymatic methods for inducing cellulose defibrillation and size reduction (Hernández-Becerra et al., 2023; Yao et al., 2023).

To the best of our knowledge, numerous studies have successfully obtained MFC via HPH processing of cellulose from various agri-waste feedstocks (Table 1). However, only a few reports have explored the use of MFC from different sources for preparing films with potential applications in the food sector. In addition, for the first time, we compare the performance of cellulosic films originating from waste biomass with a commercial solution of the same type. We hypothesize that (1) cellulose derived from different biomass sources can be used for producing films for food packaging because of comparable film-forming capabilities and functional properties compared to commercially available solutions; and (2) microfibrillated cellulose (MFC) can be effectively utilized in various food packaging applications, including as a standalone film, as a coating, or as an additive in film manufacturing.

This study builds upon our recent work (Bellesia et al., 2024), in which we evaluated the suitability of HPH for producing MFC from three biomasses of distinct origin—giant cane, *Posidonia oceanica* seagrass, and coffee silverskin. In the present work, the resulting MFC aqueous dispersions were first characterized in terms of their rheological and morphological properties to assess flow behavior and fiber dimensions, respectively. Subsequently, the optical (transparency, UV-Vis transmission, color), barrier (oxygen and water vapor), mechanical (tensile and puncture resistance, static and dynamic coefficients of friction), surface (contact angle), and morphological properties of the resulting MFC-based films were analyzed and compared with those of a high

**Table 1**
Non-exhaustive list of studies on films and coatings made from MFC produced by HPH of cellulose extracted from agri-waste biomasses.

| Source of cellulose | HPH treatment conditions | MFC-based product | Notes | Reference |
|---|---|---|---|---|
| Banana peel | P = 50 MPa, $n_C$ = 5 | Dispersion | No cytotoxicity of MFC toward Caco-2 cells up to a concentration of 500 μg/mL | Tibolla et al. (2018) |
| Rapeseed straw | P = 85–170 MPa, $n_C$ = 6 | Dispersion | A full defibrillation of pulp was pursued after 6 homogenization cycles | Svärd et al. (2019) |
| Wheat straw | P = 70 MPa, t = 30 min, $C_{CW}$ = 0.3% (w/w) | Stand-alone film | Films showed high transparency (up to 90%) and high tensile strength (up to 110 MPa) | Qi et al. (2020) |
| Okara | P = 100 – 140 MPa, $n_C$ = 3, $C_{CW}$ = 4% (w/w) | Dispersion | Increasing pressure from 100 MPa to 140 MPa improved the stability of MFC dispersions | Wu et al. (2021) |
| Carrot pomace | $n_C$ = 10, $C_{CW}$ = 1% (w/w) | Stand-alone film and coating | Spray-coating bananas with MFC dispersions curbed the enzymatic browning thereof | Amoroso et al. (2022) |
| Orange peel | P = 30 – 90 MPa, $n_C$ = 10, $C_{CW}$ = 1% (w/w) | Filler for PVA films | MFC endowed PVA films with UV-blocking capacity | Espinosa et al. (2022) |
| Cassava pulp residue | P = 138 MPa, t = 30 – 90 min, $C_{CW}$ = 0.5% (w/w) | Dispersion | The average diameter of nanofibers was reduced when extending HPH processing times | Suksri and Aht-Ong (2022) |
| Soybean residue | P = 60 MPa, $n_C$ = 15, $C_{CW}$ = 1% (w/w) | Coating on paper | MFC and AKD enhanced the mechanical stability and hydrophobicity of coated paper, respectively | Li et al. (2023) |
| Rice husk | P = 120 MPa, $n_C$ = 6 – 12, $C_{CW}$ = 1% (w/w) | Dispersion | HPH treatment increased the thermal properties of MFC dispersions | Samsalee et al. (2023) |
| Jute fiber | P = 70 MPa, $n_C$ = 15, $C_{CW}$ = 0.6% (w/w) | Stand-alone film and coating | Very low $O_2$TR values (≈ 2 $cm^3$ $m^{-2}$ $day^{-1}$) were recorded for films, whereas MFC coating extended the shelf-life of bananas and mangoes | Yu et al. (2024) |

Legend: P = pressure, $n_C$ = number of HPH cycles, t = HPH processing time, $C_{CW}$ = concentration of cellulose within water dispersion, PVA = polyvinyl alcohol, AKD = alkyl ketene dimer.

$O_2$-barrier, compostable paper-based material currently employed in food packaging.

This approach represents a promising strategy to reduce plastic consumption while delivering highly functional, bio-based materials for the food industry, in line with the circular economy principles.

## 2. Materials and methods

### 2.1. Raw materials and chemicals

Giant cane (coded as GC) cut-up was obtained from the experimental farm 'A. Menozzi' of the University of Milan (Landriano, Italy). *Posidonia oceanica* seagrass (coded as PO) was manually collected from the Sardinian shore (Alghero, Italy) and subsequently washed with tap water to remove sand. Seagrass was shipped to the laboratory in an EPS box under refrigerated conditions and delivered within 24 h. Coffee silverskin from *robusta* variety coffee beans (coded as CS) was gently donated by the "Caffè Milani" company (Lipomo, Italy). Once arrived at the laboratories, all biomasses were separately air-dried at 60°C (Memmert UF110plus, Schwabach, Germany) and further ground/sieved to yield powders of ≈ 200 μm average size (Rovera et al., 2023). All the pulverized samples were then stored in a desiccator for one week before being processed. Sylvicta® paper sheets of ≈ 42 g/m$^2$ were provided by Fedrigoni S.p.a (Verona, Italy). According to the manufacturer, Sylvicta® is a naturally-translucent, food contact material with high barrier to oxygen, odors, and mineral oils. It is obtained from virgin wood-pulp fibers that, through precision mechanical refining, are converted into MFC. Microfibrillation promotes extensive inter-fibre hydrogen bonding, resulting in a strong, dense, and clean network without the need for fillers or additives to enhance clarity. Although the available information (Fedrigoni, 2025) classifies Sylvicta® as a paper, its manufacturing process (distinct from traditional papermaking) and its physical properties (including density/porosity, transparency, flexibility, and microfibrillar nature) make it more comparable to a biopolymer film than to conventional paper. Current production of Sylvicta® is approximately 7000 tons per year. All chemicals employed in this work were of reagent grade (VWR International S.r.l., Milan, Italy) and used without further purification. Grade 230 Whatman filter paper (particle retention: 20–30 μm) for vacuum filtration was acquired from Merck KGaA (Darmstadt, Germany). All solutions were prepared using Milli-Q water with a resistivity of 18.2 MΩ·cm at 25 °C.

### 2.2. Cellulose extraction and preparation of MFC-based dispersions

Cellulose was obtained from GC, PO, and CS using the three-step method developed in our recent work (Bellesia et al., 2024). The systematic removal of hemicellulose, organic compounds and ashes, and lignin was achieved by subjecting 5 g of each biomass to NaOH hydrolysis, ethanol extraction, and final $NaClO_2$-driven bleaching, respectively. After each stage, solid/liquid separation was executed via Buchner filtration, followed by washing and drying of the residual biomass.

The dried cellulose extract obtained from each raw material was then dispersed in distilled water (1% dry weight, DW) by high-shear mixing (HSM) at 20000 rpm for 5 min using a T-25 Ultra Turrax (IKA®-Werke GmbH & Co. KG, Staufen, Germany). The so-obtained slurry underwent a 5-pass homogenization using a high-pressure system (Panda Plus, GEA Niro Soavi, Italy) working at a constant pressure of 150 MPa. To prevent excessive heating, the dispersions were cooled to 25 °C after each pass by passing through an in-house developed tube-in-tube heat exchanger positioned downstream of the homogenization valve. HSM and HPH processing conditions used in this work were set to ensure a uniform distribution and good stability of the cellulose dispersions, as indicated by preliminary results (data not shown). Cellulose dispersions were separately collected in 1 L glass bottles and stored under refrigerated conditions before analyses and film production. Because the MFC obtained from PO-derived cellulose exhibited a more pronounced hydrophilic behavior than the other samples (see the 'Results and discussion' section), we enriched the HPH-treated dispersion with beeswax (5% w/w on dry cellulose) in an attempt to improve the water resistance of the resulting films (coded as $PO_W$). The final dispersions were labeled "MFC" followed by the code of the originating source (i.e., MFC-GC, MFC-CS, MFC-PO, and MFC-$PO_W$).

### 2.3. Characterization of MFC-based dispersions

#### 2.3.1. Dry weight, density, ζ-potential, fiber length, and morphology

The dry weight of dispersions was thermogravimetrically assessed with an HS43S-MC halogen-lamp moisture-content analyzer (Mettler Toledo, Greifensee, Switzerland) set at 130°C, whereas the density was measured by a portable density meter (DMA 35, Anton Paar, Rivoli, Italy). ζ-potential was evaluated through electrophoretic light scattering (ELS) using a LitesizerTM 500 (Anton Paar, Rivoli, Italy) system at neutral pH. The tests were carried out at 25 ± 0.1 °C, with a stabilization time of 60 s, using the viscosity and refractive index of water as reference values (0.8872 cP and 1.33, respectively). The mean length of cellulose fibers was measured through the L&W fiber tester (ABB, Zurich, Switzerland). The dimensional analysis of MFC was performed using a ToscaTM 400 AFM (Anton Paar Italia S.r.l., Rivoli, Italy) in contact resonance amplitude imaging (CRAI) mode, according to the method illustrated by Rovera et al. (2023). A droplet of MFC 0.01% w/w dispersion was placed onto a mica disc (Ted Pella Inc., Redding, California) and let to dry at 40 °C for 30 min. Dimensional calculations and image editing were conducted via Tosca Analysis Software (version 7.30, Anton Paar, Graz, Austria).

#### 2.3.2. Rheological behavior

The rheological characterization of MFC-based aqueous dispersions was carried out to evaluate their behavior under shear stress, simulating conditions relevant to industrial processes such as film formation, coating, and mixing. Rheological measurements were performed in a combined motor-transducer (CMT) rheometer (DHR-2, TA Instruments, USA) using a parallel plate (40 mm in diameter) geometry at 25 ± 0.1 °C and using a solvent trap to prevent any loss of water. Data were analyzed using TRIOS software version 5.7.2 (TA Instruments, USA).

Steady-state flow tests were executed to measure the shear stress (σ, in Pa) as a function of the applied shear rate in the range 0.01–1000 s$^{-1}$. Data from the flow curves (shear stress vs. shear rate) were fitted using the Herschel-Bulkley model (Eq.1):

$$\sigma = \sigma_0 + k\dot{\gamma}^n \quad (1)$$

where $\sigma_0$ is the yield stress (Pa), k is the consistency index (Pa · s$^n$), $\dot{\gamma}$ is the shear rate (s$^{-1}$), and n is the dimensionless flow behavior index. At last, the apparent viscosity ($n_{APP}$, in Pa · s) of all dispersions was plotted against the shear rate.

Dynamic mechanical investigations focused on the mechanical spectra of MFC-based aqueous dispersions. The linear viscoelastic region (LVR) for all MFC dispersions was determined by performing amplitude strain sweep tests. To this end, the amplitude was changed from 0.001% to 1000% at a constant frequency of 1 Hz. For the frequency sweep tests, a strain amplitude of 0.5% was selected, whereas the frequency varied between 0.01 Hz and 100 Hz. The elastic (G', in Pa) and viscous (G″, in Pa) components of the complex modulus (G*, in Pa) were finally plotted against the frequency.

### 2.4. Film formation

For film obtainment, the aqueous dispersions were poured into square PS Petri dishes (12 × 12 cm$^2$) and subsequently conditioned first at 60 °C for 3 h and then at 25 °C in a desiccator for additional 24 h. To make a proper comparison with the commercial paper-based solution (Sylvicta®), films at a standardized thickness of 40 μm were produced. The thickness of films was determined using a micrometer (Dialmatic DDI030M, Bowers Metrology, Bradford, UK) with an accuracy of 1 μm at 10 random points.

All film samples were stored in a climatic chamber at 25°C and 50% RH before analyses.

### 2.5. Characterization of the films

#### 2.5.1. Optical properties

Transparency ($T_{550}$, in %) of films was measured by a high-performance UV-Vis spectrophotometer (Lambda 650, PerkinElmer, Waltham, MA, USA) in accordance with ASTM D1746. Transmission spectra allowed to determine the UV-screening ability of films within the wavelength range of 200 – 400 nm (Mengozzi et al., 2024). Color assessment was performed in the wavelength range of 400 – 800 nm operating in reflectance mode, using a D65 illuminant and 10° observer angle.

#### 2.5.2. Oxygen and water vapor barrier properties

The barrier properties of the cellulosic films against oxygen and water vapor permeation were investigated on a 50 $cm^2$ surface sample using a TotalPerm permeability analyzer (ExtraSolution®Srl, Capannori, Italy) equipped with an electrochemical sensor for oxygen and an infrared sensor for water vapor. The oxygen transmission rate [$O_2TR$, in $cm^3$ (STP) $m^{-2}$ $day^{-1}$] was determined according to the isostatic method at 23 °C and at 0% and 50% RH, according to ASTM D3985 and ASTM F1927, respectively. A carrier flow ($N_2$) of 10 mL $min^{-1}$ and a 1 atm $O_2$ partial pressure difference between the two sides of the specimen were applied. The water vapor transmission rate (WVTR, in g $m^{-2}$ $day^{-1}$) was measured according to ASTM F1249, with a carrier flow ($N_2$) of 10 mL $min^{-1}$ at 23°C and 65% RH.

#### 2.5.3. Mechanical properties

Mechanical features of films were assessed using a dynamometer (model Z005, Zwick Roell, Ulm, Germany) fitted with a 5-kN load cell (Carullo et al., 2023a). Elastic modulus ($E_T$, in GPa), elongation at break ($\varepsilon_B$, in %), and tensile strength (TS, in MPa) were measured through a tensile test on film strips 12 cm in length with a specimen gage length of 10 cm and 1.5 cm in width, according to ASTM D882.

Puncture tests were conducted according to ASTM F1306, using specimens with a 6-cm diameter punctured by a hemispherical (biaxial stress) probe with a 3.2-mm diameter. Load cell nominal capacity and probe speed during the test were set at 100 N and 25 mm/min, respectively. The samples' resistance to puncturing was evaluated in terms of elastic modulus ($E_C$, in MPa), maximum force ($F_{MAX}$, in N), and work of rupture (W, in mJ).

Static ($\mu_S$) and dynamic ($\mu_D$) coefficients of friction (COF) were determined according to ASTM D1894 in typical "film vs. film" and "film vs. metal" configurations. The former allowed for the evaluation of the friction opposing the motion of each type of material against itself. The latter was intended to simulate the friction between the material web and the metallic parts of the equipment used during the manufacturing process (Farris, 2018). For each parameter, the final mean of the results was calculated from at least five replicates.

The software TestXpert V10.11 was used for data analysis in all three mechanical tests.

#### 2.5.4. Morphological properties

Morphological information of films was gathered using a table-top scanning electron microscope (SNE-ALPHA, SEC Co., Korea) working at an accelerating voltage of 10 kV. Rectangular specimens of films were first mounted on metallic stubs covered with carbon tape and subsequently metalized with gold to an approximate thickness of 5 nm using an MCM-100 ion sputter coater (SEC Co., Korea). SEM micrographs of the top surface and cross-section were collected at 250 × and 5000 × magnifications, respectively. The topography of the films surface was investigated using a ToscaTM 400 AFM (Anton Paar Italia Srl, Rivoli, Italy) in contact resonance amplitude imaging (CRAI) mode (Chandrasekar et al., 2024), using an Arrow-FMR-10 Force Modulation probe (Nanoworld, Neuchatel, Switzerland) featuring a rectangular cantilever with a triangular free end and a tetrahedral tip with a typical height of 10–15 μm and radius of curvature of ≈ 10 nm. The cantilever has a spring constant and resonance frequency of 2.8 N $m^{-1}$ and 75 kHz, respectively. For the analyses, specimens (1 × 1 $cm^2$) of dried films were placed onto a highest-grade V1 AFM mica disc (Ø = 20 mm; mean roughness < 2 nm) (Nanovision srl, Brugherio, Italy) and scanned. Root mean square roughness (Sq, in nm) and image editing were conducted via Tosca Analysis Software (version 7.30, Anton Paar, Graz, Austria).

#### 2.5.5. Surface properties

Contact angle analysis was conducted using an optical contact angle apparatus (OCA 15 Plus, Data Physics Instruments GmbH, Filderstadt, Germany) equipped with a high-resolution CCD camera and a high-performance digitizing adapter. SCA20 software (Data Physics Instruments GmbH, Filderstadt, Germany) was used for data collection and contact angle measurement. Rectangular specimens (5 × 2 $cm^2$) were safely positioned in a flat orientation using a sample holder equipped with parallel clamping jaws. The evolution of the contact angle of water in air ($\theta$, in °) was measured using the sessile drop method at constant thermo-hygrometric conditions, as previously described by Ghaani et al. (2024). More specifically, a droplet of 4 ± 0.5 μL of Milli-Q water (18.2 MΩ·cm) was gently placed on the cellulose films from a height of 1 cm above their surface to ensure consistency between each measurement (Çavdaroğlu et al., 2023). The contact angle values over time were measured using a software-assisted image-processing procedure with a video-capturing system, starting from the deposition of the drop ($t_0 = 0$ s) to up to 30 s ($t_{30} = 30$ s). A minimum of 10 droplets were examined for each cellulosic sample on both the left and right sides and the resulting mean $\theta$ values were then used for the following discussion.

### 2.6. Statistical analysis

All experiments and analyses were repeated three times unless otherwise specified. The mean value and standard deviation (SD) were calculated from the experimental data. Statistically significant differences among the averages were evaluated using a one-way analysis of variance (ANOVA) and Tukey's test ($p \leq 0.01$). Statistical analysis was carried out using IBM SPSS Statistics 20 software (IBM Corp., Armonk, New York, USA).

## 3. Results and discussion

### 3.1. ζ-potential and morphology of MFC-based dispersions

ζ-potential is a key indicator of colloidal stability and it is widely used to predict the tendency of a suspension or dispersion to undergo aggregation and precipitation. Generally, colloidal systems with ζ-potential higher than |30| mV are considered kinetically stable, whereas ζ-potential lower than |30| mV produce less stable colloidal dispersions, which are prone to aggregation, flocculation, and phase separation over time (Carullo et al., 2023b). MFC dispersions exhibited very similar ζ-potential values (Table 2), with the exception of MFC-GC, which showed a slightly lower, though significant, stability ($p < 0.01$). Besides inherent properties such as the surface charge of cellulose (Farris et al., 2012), ζ-potential differences could be attributed to the significantly ($p < 0.01$) greater length of the cellulose fibers in GC (0.647 ± 0.01 mm) compared to CS (0.333 ± 0.01 mm) and PO (0.318 ± 0.01 mm) biomasses after the HPH process (Table 2). Plausibly, under constant HPH conditions (P = 150 MPa, $n_P = 5$), longer nanofibers were obtained after the mechanical miniaturization of cellulose from GC. According to Tibolla et al. (2018), size reduction through HPH can maximize repulsive forces among the nanofibers and give rise to enough surface charges to stabilize the system. In addition, compositional differences (such as residual hemicellulose or lignin) between MFC-GC and MFCs obtained from CS and PO may influence the surface chemistry of the matrix, thereby affecting the final dispersion stability (Bellesia et al., 2024).

**Table 2**
Thickness and root mean square surface roughness of MFC films obtained in this study and Sylvicta®. Dry weight, density, ζ- potential, and fiber length of MFC aqueous dispersions.

| | Films | | Dispersions | | | |
|---|---|---|---|---|---|---|
| Sample | δ [μm] | Sq [nm] | Dry weight [%] | Density [kg m$^{-3}$] | ζ-potential [mV] | Fiber length (mm) |
| MFC-GC | 40 ± 3$^{a}$ | 824 ± 53$^{b}$ | 1.01 ± 0.02$^{a}$ | 1002 ± 13$^{a}$ | -20.9 ± 0.4$^{a}$ | 0.647 ± 0.01$^{a}$ |
| MFC-CS | 39 ± 3$^{a}$ | 433 ± 69$^{b}$ | 0.99 ± 0.01$^{a}$ | 997 ± 15$^{a}$ | -31.9 ± 1.1$^{bc}$ | 0.333 ± 0.01$^{b}$ |
| MFC-PO | 39 ± 3$^{a}$ | 653 ± 27$^{b}$ | 1.04 ± 0.02$^{a}$ | 1000 ± 21$^{a}$ | -28.8 ± 0.9$^{b}$ | 0.318 ± 0.01$^{b}$ |
| MFC-PO$_W$ | 40 ± 4$^{a}$ | 605 ± 92$^{b}$ | 1.02 ± 0.01$^{a}$ | 997 ± 10$^{a}$ | -35.0 ± 1.2$^{c}$ | / |
| Sylvicta® | 42 ± 3$^{a}$ | 2195 ± 247$^{a}$ | N.A. | N.A. | N.A. | N.A. |

Results are expressed as means ± standard deviation. For each investigated parameter, values with different superscript letters within the same column are significantly different ($p < 0.01$). Legend: N.A. – Not applicable.

In terms of morphology, Fig. 1 shows that an entangled, web-like network of nanofibrils was obtained after the HPH treatment, in full agreement with recent findings (Ortiz et al., 2018; Wei et al., 2023; Yu et al., 2024). In addition, the thickness of the nanofibrils never exceeded 100 nm, while their length was in the micrometric range. Partially in contrast with our results, Kraft vegetal cellulose pulp homogenized at 80 MPa for 18 passes yielded fibers with an average diameter > 146 nm (Hernández-Becerra et al., 2023). This discrepancy could be due to the different HPH treatment severity and the type of dispersing agent used, as well as the biomass origin.

### 3.2. Rheological properties of MFC-based dispersions

The flow behavior of MFC and the shear-induced organization of its network are critical factors for rheological modifications and processing performance. The flow curve for each MFC aqueous dispersion was analyzed to determine the apparent viscosity as a function of the shear rate (Fig. 2a). The experimental data were further fitted using the Herschel-Bulkley model.

The flow behavior index (n) was less than 1 for all samples (Table 3), confirming the non-Newtonian shear-thinning behavior typical of cellulose derivative dispersions. This result is consistent with previous findings (Cinar Ciftci et al.,2020; Kumar et al., 2016) and can be attributed to the reduction in intermolecular interactions and the

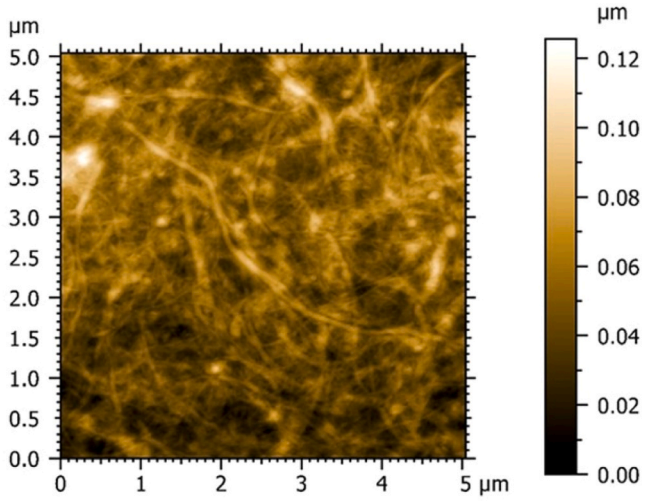


**Fig. 1.** AFM height image of MFC from PO-derived cellulose.

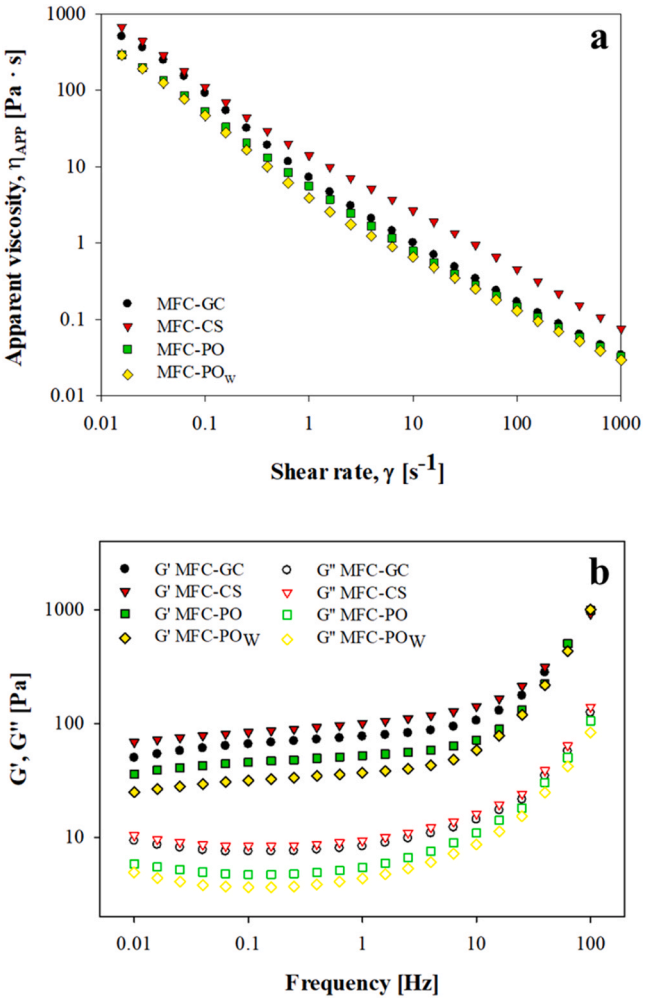


**Fig. 2.** Curves of (a) apparent viscosity vs. shear rate and (b) storage-loss moduli vs. frequency for the MFC aqueous dispersions from tested biomasses.

**Table 3**
Flow behavior index (n), consistency index (k), and yield stress ($\sigma_0$) of MFC-based aqueous dispersions from tested biomasses, obtained from the flow curves data regression by the Herschel–Bulkley model (Eq. 1).

| Sample | n [-] | K [Pa s$^{n}$] | $\sigma_0$ [Pa] | $R^2$ |
|---|---|---|---|---|
| MFC-GC | 0.49 ± 0.01$^{a}$ | 0.93 ± 0.05$^{b}$ | 7.61 ± 0.05$^{a}$ | 0.99 |
| MFC-CS | 0.26 ± 0.01$^{c}$ | 11.93 ± 0.11$^{a}$ | 4.36 ± 0.07$^{b}$ | 0.99 |
| MFC-PO | 0.45 ± 0.01$^{b}$ | 1.30 ± 0.05$^{b}$ | 4.47 ± 0.05$^{b}$ | 0.99 |
| MFC-PO$_W$ | 0.46 ± 0.01$^{b}$ | 1.08 ± 0.09$^{b}$ | 3.75 ± 0.08$^{c}$ | 0.99 |

Results are expressed as means ± standard deviation. For each investigated parameter, values with different superscript letters within the same column are significantly different ($p < 0.01$).

orientation of nanofibers under shear (Wu et al., 2021). Notably, MFC-CS exhibited a moderate yield stress ($\sigma_0 \approx 4.4$ Pa), the highest consistency index ($k \approx 12$ Pa s$^{n}$) and the lowest flow behavior index ($n \approx 0.26$) ($p < 0.01$), indicating a dense, highly entangled fibril network with soft gel-like behavior. Under gentle stirring, the dispersion appeared thick and resistant; however, when subjected to higher shear, its viscosity decreased sharply, enabling flow before rebuilding structure at rest (Fig. 2a). This shear-thinning and thixotropic behavior is characteristic of finely fibrillated, high-surface-area networks in which water is effectively immobilized within a three-dimensional nanofiber web.

The MFC-GC dispersion exhibited opposite rheological behavior. Despite its lowest viscosity at low shear ($k \approx 0.9$ Pa s$^{n}$) and only

moderate shear-thinning ($n \approx 0.49$), it required the highest yield stress to initiate flow ($\sigma_0 \approx 7.6$ Pa). This combination of rheological parameters indicates a looser, coarser fibril network that nevertheless forms strong interparticle contacts, possibly due to residual lignin or other cell-wall components acting as 'molecular glue'. Consequently, MFC-GC effectively resists sagging or sedimentation at rest, but once the critical stress is exceeded, it remains comparatively fluid during processing.

MFC-PO and MFC-$PO_W$ displayed intermediate rheological behavior compared to MFC-CS and MFC-GC. Their flow indices ($n \approx 0.45$–$0.46$) and consistency values ($k \approx 1$ Pa $s^n$) indicate moderate pseudoplasticity with a low-to-medium viscosity baseline. The slightly lower yield stress of $PO_W$ ($\approx 3.8$ Pa) compared to PO ($\approx 4.5$ Pa) likely reflects the presence of beeswax, which weakens interparticle interactions without significantly affecting fibrillation. This supports the role of wax as a lubricant, reducing the initial flow resistance and enhancing flowability. As a result, the dispersions can be readily pumped or sprayed while retaining sufficient structural strength to prevent phase separation during storage.

In summary, the observed rheological differences can be attributed to intrinsic biomass characteristics rather than processing history: finer fibril morphology increases k and decreases n (as seen in CS), stronger inter-fibril interactions elevate $\sigma_0$ (GC), and selective removal of lignin and hemicellulose modulates $\sigma_0$ without substantially affecting overall viscosity (PO versus $PO_W$). Thus, the same homogenization protocol can produce markedly different flow profiles depending on feedstock chemistry and microstructure, highlighting that, for MFC systems, fiber origin is as critical as processing energy in determining end-use performance.

In view of the potential use of MFC for food packaging applications, MFC-CS is best suited for applications requiring pronounced shear thinning behavior and rapid structural recovery—i.e., formulations that must remain solid at rest but flow under applied stress. This rheological profile is especially advantageous for applications such as the production of stand-alone films. MFC-GC, with its high yield stress but moderate viscosity, is more suitable for coatings or suspensions that must remain stable during storage yet spread uniformly during application, consistent with reports of MFC dispersions used as paper/plastic coatings (Jin et al., 2021; Lengowski et al., 2023; Li et al., 2023) applied via slot-die or reverse-gravure techniques (Schiessl et al., 2023). MFC-PO and MFC-$PO_W$, showing intermediate behavior, are well suited as rheological modifiers when a balance between processability and stability is required.

The rheology of MFC dispersions is closely related to morphology factors including size, shape, and the aspect ratio of MFC and other components (Cinar Ciftci et al., 2020). Specifically, MFC consists of a mixture of coarse particles and bundles of cellulose nanofibrils, exhibiting relatively low surface charge and a broad size distribution across both micro- and nano-scales. In water, MFC can form highly entangled fibrillar networks that exhibit a predominantly elastic behavior, as gathered from the frequency-sweep tests (Fig. 2b). The fact that $G'$ exceeded $G''$, with only mild frequency dependence across the operational window, confirms that all MFC dispersions behaved as physical gels within the linear viscoelastic regime. Below ~10 Hz, a plateau or weak-gel region was observed, where the networks stored most of their elastic energy, an important feature for comparing formulations and predicting long-term stability. This behavior is consistent with the pseudoplastic flow curves, which showed finite yield stress and pronounced shear thinning. In line with the flow analysis, the dynamic mechanical results further support the presence of a percolated fibrillar network that is only partially disrupted under moderate deformation. The experimental evidence that MFC-CS exhibits the highest $G'$ up to 10 Hz is consistent with its very high consistency index (k) and low flow behavior index (n). A dense, highly entangled micro/nano network can store more elastic energy (high $G'$) and resist flow (high $\eta_{APP}$) until higher shear rates are applied. In the steady-shear data, MFC-GC showed the highest yield stress but the lowest k value, and its lower $G'$ plateau compared to MFC-CS is therefore not contradictory: $\sigma_0$ represents the stress required to disrupt the network, while small-amplitude $G'$ reflects the stiffness of the intact network under infinitesimal strain. A network with strong but relatively sparse junctions (e.g., contacts mediated by residual lignin) can yield a high $\sigma_0$ despite a moderate linear-viscoelastic modulus. MFC-PO and MFC-$PO_W$ exhibited $G'$ values below MFC-CS but comparable to each other, consistent with their nearly identical n and k values and only slightly different yield stresses. The presence of beeswax in $PO_W$ marginally reduced $\sigma_0$ without appreciably altering the linear viscoelastic response, again in agreement with the flow analysis (Fig. 2a).

The interpretation of the mechanical spectra is consistent with the flow-curve analysis. The dynamic data confirm that: i) MFC-CS forms the densest and most elastic network, thinning rapidly under shear; ii) MFC-GC exhibits a network with strong junctions (high $\sigma_0$) but lower linear stiffness; and iii) MFC-PO and MFC-$PO_W$ display intermediate, gel-like behavior. In addition, the pronounced difference between $G'$ and $G''$ and the minimal frequency dependence observed across all samples clearly demonstrate the gel-like nature of MFC dispersions, in agreement with previous reports (Rantanen et al., 2015; Yao et al., 2023).

### 3.3. Functionality of stand-alone films

#### 3.3.1. Optical properties

Concerning the optical properties of the films, Table 4 shows that an increasing trend in $T_{550}$ and L* of films was recorded in the following order: MFC-GC<MFC-CS<MFC-PO, whereas a* and b* coordinates displayed an opposite behavior. No statistical differences were observed between MFC-PO and MFC-$PO_W$ ($p > 0.01$), indicating that the addition of beeswax to HPH-treated dispersions at the concentration tested in this work did not impair the optical properties of the final film.

Films obtained from CS and PO exhibited transparency and lightness comparable to Sylvicta® ($p > 0.01$). However, slight but significant ($p < 0.01$) differences in terms of a* and b* among these samples were observed, with a higher yellowish component (+ b*) observed for MFC-GC and MFC-CS films (Table 4). MFC-GC films, in particular, appeared opaque and showed a lower transparency (Fig. 3a) compared to the other samples, which allowed clearer visibility of the icon placed behind them. A strong negative linear correlation was observed between cellulose fiber length and the optical properties of MFC films ($R^2 = 0.92$, data not shown). These results suggest that tailoring the size of cellulose nanofibrils allows control over light–material interaction phenomena. This hypothesis is supported by Liu et al. (2020), who isolated cellulose nanofibrils from bleached sugarcane bagasse using endoglucanase-assisted mechanical grinding.

Increasing enzyme dosage during pre-treatment enhanced nanofibrils miniaturization and improved the optical properties of the resulting films. The authors attributed this effect to the tight entanglement of smaller nanofibrils into denser structures that reduced light scattering, thereby producing films with high transparency and low haze. Similarly, Thongsomboon et al. (2023) reported that film transparency is strongly influenced by fiber size: smaller fibers promote transparency, whereas larger fibers yield opaque films.

All MFC-based films demonstrated good UV-blocking capability, as indicated by the sharp decrease in transmittance below 400 nm

**Table 4**
Transparency and color coordinates for all films tested in this work.

| Sample | $T_{550}$ [%] | L* | a* | b* |
|---|---|---|---|---|
| MFC-GC | $54.8 \pm 1.4^{c}$ | $79.70 \pm 1.67^{c}$ | $0.51 \pm 0.03^{c}$ | $2.59 \pm 0.06^{c}$ |
| MFC-CS | $75.5 \pm 4.4^{b}$ | $88.84 \pm 2.00^{b}$ | $0.23 \pm 0.06^{b}$ | $2.94 \pm 0.63^{c}$ |
| MFC-PO | $84.9 \pm 1.2^{a}$ | $93.86 \pm 0.36^{a}$ | $0.05 \pm 0.02^{a}$ | $1.06 \pm 0.30^{b}$ |
| MFC-$PO_W$ | $85.2 \pm 1.9^{a}$ | $93.59 \pm 1.37^{a}$ | $0.02 \pm 0.01^{a}$ | $0.68 \pm 0.14^{b}$ |
| Sylvicta® | $80.4 \pm 0.2^{ab}$ | $92.04 \pm 0.09^{ab}$ | $0.31 \pm 0.01^{b}$ | $-0.63 \pm 0.04^{a}$ |

Results are expressed as means ± standard deviation. For each investigated parameter, values with different superscript letters within the same column are significantly different ($p < 0.01$).

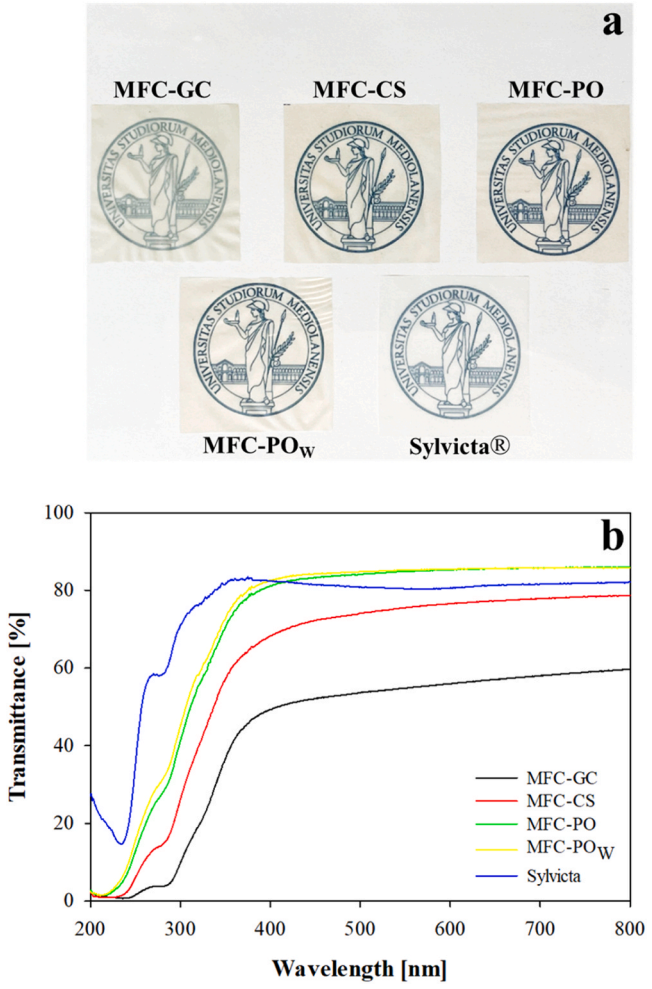


**Fig. 3.** Digital photos (a) and UV-Vis transmission spectra (b) of all films investigated in this work.

(Fig. 3b). This property is essential for protecting food products susceptible to UV-induced oxidation and discoloration (Amoroso et al., 2022; Mengozzi et al., 2024). Comparable findings were reported by Yu et al. (2024) for HPH-derived MFC from jute fibers, which produced films combining strong UV-shielding with high visible-light transparency. The authors attributed this effect to chromophoric noncellulosic impurities (e.g., phenolic groups in lignin) that absorb UV light, consistent with our previous results (Bellesia et al., 2024). Notably, all films from HPH-treated cellulose dispersions outperformed the commercial benchmark in terms of UV-barrier properties (Fig. 3b).

### 3.3.2. *Barrier properties*

The overall performance of MFC samples as barrier to oxygen and water vapor is greatly affected by the thermo-hygrometric conditions. As reported in Table 5, under dry conditions, MFC-GC, MFC-CS, MFC-PO, and Sylvicta® films acted as full barrier materials against oxygen, owing to the compact and dense network of microfibrils generated upon drying. At 50% RH, MFC-CS films still behaved as impermeable material to oxygen. This performance supports the findings arising from the rheological tests, which indicated that MFC-CS forms the densest network ensuing from the high entanglement of cellulose fibrils. The oxygen barrier performance slightly decreased at 50% RH for MFC-GC, MFC-PO, and Sylvicta® films, although the $O_2TR$ values were still below 1 $cm^3$ (STP) $m^{-2}$ $day^{-1}$ (Table 5). The detrimental impact of humidity was due to the plasticizing effect of water molecules absorbed by biopolymers, which led to an increased chain mobility and intermolecular

**Table 5**
$O_2TR$ and WVTR values for all films tested in this work.

| Sample | $O_2TR_{23°C\text{-}0\%\ RH}$ [$cm^3$ (STP) $m^{-2}$ $day^{-1}$] | $O_2TR_{23°C\text{-}50\%\ RH}$ [$cm^3$ (STP) $m^{-2}$ $day^{-1}$] | $WVTR_{23°C\text{-}65\%\ RH}$ [g $m^{-2}$ $day^{-1}$] |
|---|---|---|---|
| MFC-GC | < LDL | 0.95 ± 0.06[a] | 56.40 ± 3.47[b] |
| MFC-CS | < LDL | < LDL | 55.68 ± 4.18[b] |
| MFC-PO | < LDL | 0.27 ± 0.03[c] | 54.62 ± 5.14[b] |
| MFC-PO$_W$ | > UDL | > UDL | > UDL |
| Sylvicta® | < LDL | 0.44 ± 0.05[b] | 87.08 ± 4.13[a] |

Results are expressed as means ± standard deviation. For each investigated parameter, values with different superscript letters within the same column are significantly different ($p < 0.01$).
LDL = lower detection limit [0.01 $cm^3$ (STP) $m^{-2}$ $day^{-1}$ for $O_2TR$], UDL = upper detection limit [1000 $cm^3$ (STP) $m^{-2}$ $day^{-1}$ for $O_2TR$, 100 g $m^{-2}$ $day^{-1}$ for WVTR].

free volume (Wei et al., 2023). Regardless of the humidity level, the MFC-PO$_W$ film showed an extremely high permeability to oxygen, with $O_2TR$ values above the upper detection limit of the instrument (Table 5). This can be attributed to the hydrophobic nature of beeswax, which plausibly caused phase segregation and the occurrence of discontinuities in the H-bonding framework of the MFC network (Klangmuang & Sothornvit, 2016).

Concerning the permeability to water vapor, medium-high WVTR values were recorded for all films (Table 5), which is plausibly explained considering the hydrophilic nature of MFC. Once again, the only exception concerned the MFC-PO$_W$ sample, with WVTR above the upper instrumental detection limit, clearly showing that the addition of a hydrophobic component (beeswax) is not sufficient to control the permeation of water vapor in a hydrophilic film. Under tropical conditions (38 °C and 90% RH), none of the samples maintained any barrier capacity against water vapor, and all final WVTR values were above the upper detection limit of the instrument. These data are consistent with the results previously reported, which demonstrated the potential of MFC to generate films suitable for specific food applications, such as low water activity and oxygen-sensitive foods (Amoroso et al., 2022; Dou et al., 2021; Qi et al., 2020; Yu et al., 2024).

### 3.3.3. *Mechanical properties*

Tensile, puncture, and friction behavior of the MFC films and the commercial reference is summarized in Table 6. All samples exhibited tensile parameters consistent with those of MFC films derived from other agri-food wastes and plant residues, such as cereal bran, carrot pomace, wheat straw, bast fibers, and eucalyptus pulp (Aguiló-Aguayo et al., 2024; Amoroso et al., 2022; Qi et al., 2020; Wei et al., 2023; Yu et al., 2024). Specifically, no statistical differences ($p > 0.01$) were observed among MFC-GC, MFC-CS, MFC-PO, and Sylvicta® films with respect to $E_T$ values. In contrast, MFC-PO$_W$ exhibited significantly lower stiffness, which can be attributed to the presence of beeswax that reduces the internal cohesiveness of the primary MFC network at the intermolecular level. The values of $\varepsilon_B$ and TS varied significantly ($p < 0.01$) depending on the sample. Notably, the highest values for both parameters were found in MFC-CS films, confirming previous findings that their highly dense and compact network allows greater elongation and resistance to higher loads before rupture.

In the puncture test, MFC-based films exhibited greater resistance to penetration than the reference material ($p < 0.01$, Table 6), with $E_P$ and $F_{MAX}$ values that approached those reported for a 25-μm oriented PE film (Carullo et al., 2023a). However, the limited extensibility of the films resulted in rapid rupture under compression, thereby reducing the area under the force–distance curve (W).

In the friction tests, all MFC films exhibited static and dynamic coefficients between 0.2 and 0.4 in both configurations (i.e., film vs. film and film vs. metal) (Table 6). These values are considered acceptable at

**Table 6**
Main parameters obtained from the tensile, puncture, and friction tests carried out on all films tested in this work.

| | Tensile parameters | | | Puncture parameters | | |
|---|---|---|---|---|---|---|
| Sample | $E_T$ [GPa] | $\varepsilon_B$ [%] | TS [MPa] | $E_P$ [MPa] | $F_{MAX}$ [N] | W [mJ] |
| MFC-GC | $8.0 \pm 0.5^{a}$ | $2.5 \pm 0.7^{b}$ | $93 \pm 10^{a}$ | $6.8 \pm 1.3^{a}$ | $9.1 \pm 1.4^{a}$ | $5.8 \pm 0.7^{ab}$ |
| MFC-CS | $7.8 \pm 1.4^{a}$ | $3.1 \pm 0.5^{a}$ | $106 \pm 28^{a}$ | $6.5 \pm 0.3^{a}$ | $8.9 \pm 0.4^{a}$ | $5.0 \pm 0.5^{ab}$ |
| MFC-PO | $8.0 \pm 1.1^{a}$ | $1.0 \pm 0.2^{c}$ | $67 \pm 12^{b}$ | $5.9 \pm 0.7^{ab}$ | $8.9 \pm 2.3^{a}$ | $5.9 \pm 2.3^{ab}$ |
| MFC-$PO_W$ | $5.8 \pm 0.6^{b}$ | $0.6 \pm 0.1^{c}$ | $39 \pm 15^{c}$ | $4.5 \pm 0.1^{bc}$ | $9.9 \pm 0.7^{a}$ | $7.2 \pm 0.6^{a}$ |
| Sylvicta® | $9.9 \pm 1.1^{a}$ | $1.6 \pm 0.2^{bc}$ | $115 \pm 9^{a}$ | $3.7 \pm 0.3^{c}$ | $4.9 \pm 0.7^{b}$ | $2.7 \pm 0.6^{b}$ |

| | Friction parameters | | | |
|---|---|---|---|---|
| | Film vs. film | | Film vs. metal | |
| Sample | $\mu_S$ | $\mu_D$ | $\mu_S$ | $\mu_D$ |
| MFC-GC | $0.35 \pm 0.03^{a}$ | $0.31 \pm 0.01^{a}$ | $0.27 \pm 0.01^{a}$ | $0.20 \pm 0.01^{a}$ |
| MFC-CS | $0.26 \pm 0.01^{a}$ | $0.21 \pm 0.02^{b}$ | $0.23 \pm 0.02^{a}$ | $0.16 \pm 0.01^{b}$ |
| MFC-PO | $0.29 \pm 0.01^{a}$ | $0.25 \pm 0.01^{ab}$ | $0.24 \pm 0.01^{a}$ | $0.19 \pm 0.01^{a}$ |
| MFC-$PO_W$ | $0.33 \pm 0.04^{a}$ | $0.26 \pm 0.04^{ab}$ | $0.24 \pm 0.01^{a}$ | $0.19 \pm 0.01^{a}$ |
| Sylvicta® | $0.13 \pm 0.01^{b}$ | $0.04 \pm 0.01^{c}$ | $0.13 \pm 0.02^{b}$ | $0.07 \pm 0.01^{c}$ |

Results are expressed as means ± standard deviation. For each investigated parameter, values with different superscript letters within the same column are significantly different ($p < 0.01$).

the industrial level for in-line operations such as winding and unwinding (Carullo et al., 2023a). In contrast, the commercial film showed significantly lower values. Excluding the presence of hydrophobic components in the Sylvicta® formulation, this effect is plausibly attributable to topographical differences, such as surface roughness, as discussed in the next section. In general, higher surface roughness reduces the number of contact points between a material and either itself or a metal surface, thereby leading to a significant reduction in interfacial friction (Cozzolino et al., 2016).

### 3.3.4. Morphological properties

The morphological and topographical features of the films were evaluated by SEM (Fig. 4) and AFM (Fig. 5), respectively. The surfaces appeared compact and relatively uniform, while the cross-sections exhibited an irregular lamellar structure (Fig. 4), consistent with previous reports (Qi et al., 2020; Zhang et al., 2023). Cellulose fibrils were evident only in MFC-GC and Sylvicta® samples. AFM analyses allowed quantification of film surface roughness, as reported in Table 2. The highest Sq value was measured for Sylvicta®, followed by the films prepared using MFC-GC. We hypothesize that these high Sq values are related to the size and aggregation state of MFC bundles, as evident in the AFM images, particularly for Sylvicta® (Fig. 5e). For the other MFC samples, no statistically significant differences were observed in Sq values, which were consistently lower than those measured for MFC-GC and Sylvicta®. This result is likely attributable to the presence of impurities (e.g., lignin and hemicellulose residues) that exert a filling effect on the overall network structure (Yu et al., 2024). In the case of the MFC-$PO_W$ film, in particular, the smooth and even surface can also be ascribed to the presence of wax in the MFC-PO dispersion (Fig. 4).

### 3.3.5. Surface properties

Investigating the wettability phenomena is crucial to understand the interface phenomena between the liquid (water) and the film's surface (Jiang et al., 2025). This will allow to predict the behavior of the cellulosic materials for practical uses, including food packaging applications, where phenomena such as spreading or absorption of water may dictate the success or failure of the final material during converting operations (e.g., printing, lamination, and coating) and service life of the final material (e.g., resistance to water absorption).

The interaction between the film surface and water is depicted in Fig. 6. The initial ($t_0$) contact angle varied markedly among samples, with the highest values recorded for Sylvicta® ($\theta = 115.8^{\circ} \pm 9.6$) and MFC-GC films ($\theta = 96.4^{\circ} \pm 7.9$), whereas the lowest values were measured for MFC-CS ($\theta = 84.6^{\circ} \pm 8.2$), MFC-PO ($\theta = 53.5^{\circ} \pm 6.7$), and MFC-$PO_W$ ($\theta = 60.6^{\circ} \pm 7.4$) films. Interestingly, this trend follows the order of Sq values obtained by AFM (Table 2), strongly suggesting that the very first interaction at the solid/liquid interface is governed by topographical reasons—the higher the roughness, the higher the contact angle. This effect is likely related to differences in the fibrillation degree of the cellulose used to prepare MFC (Arafat et al., 2025). However, as soon as the water droplet is released on the film surface, the contact angle decreased abruptly for all films except MFC-$PO_W$. This decrease is explained by the polar surface chemistry of the materials, which promotes strong solid-liquid affinity and thus spreading, a phenomenon typical of polar surfaces (Farris et al., 2011). The duration of the spreading phase (i.e., the descending part of the curves) differed across films: approximately 1 s for Sylvicta® and MFC-PO films, ca. 2.5 s for the MFC-GC sample, and ca. 17 s for the MFC-CS film, most likely reflecting compositional differences. As noted above, spreading did not occur on the MFC-$PO_W$ surface, corroborating the crucial role of surface chemistry in this process.

The descending part of the curve was followed by a rising part, in which the contact angle increased. This behavior is characteristic of polar and relatively porous materials that absorb water. This second phenomenon (absorption) has been explained in terms of water percolation into the porous and fibrous

surface, causing swelling that lifts the water droplet and produces an apparent increase in contact angle (see Supplementary Material) (Mayrhofer et al., 2023). Absorption was more pronounced in Sylvicta®, MFC-PO, and MFC-$PO_W$ films, while less evident in MFC-CS and MFC-GC films, suggesting that the latter may be more suitable for food packaging applications requiring resistance to medium-high relative humidity. None of the tested films, however, proved suitable for direct contact with water, for which a functional water barrier layer (coating) would be necessary.

## 4. Conclusions

In this study, three biomasses of different origin and composition were successfully valorized through cellulose extraction followed by HPH-assisted miniaturization to microfibrillated cellulose (MFC).

The results demonstrated that the origin of the biomass significantly influences the rheological properties of the resulting MFC aqueous dispersions. Notably, application of an identical homogenization protocol yielded markedly different flow behaviors, suggesting that MFC dispersions can be selectively tailored for various manufacturing applications (e.g., films, coatings, or as additives/fillers), depending on the biomass source. Furthermore, MFC stand-alone films exhibited an exceptional oxygen barrier performance under dry and intermediate RH conditions, whereas the incorporation of a waxy additive did not enhance the water vapor barrier performance of the films; in fact, it negatively impacted the pristine oxygen barrier performance of the unmodified film. Films also showed high stiffness and good resistance to punctural stresses, whereas the transparency and lightness followed a

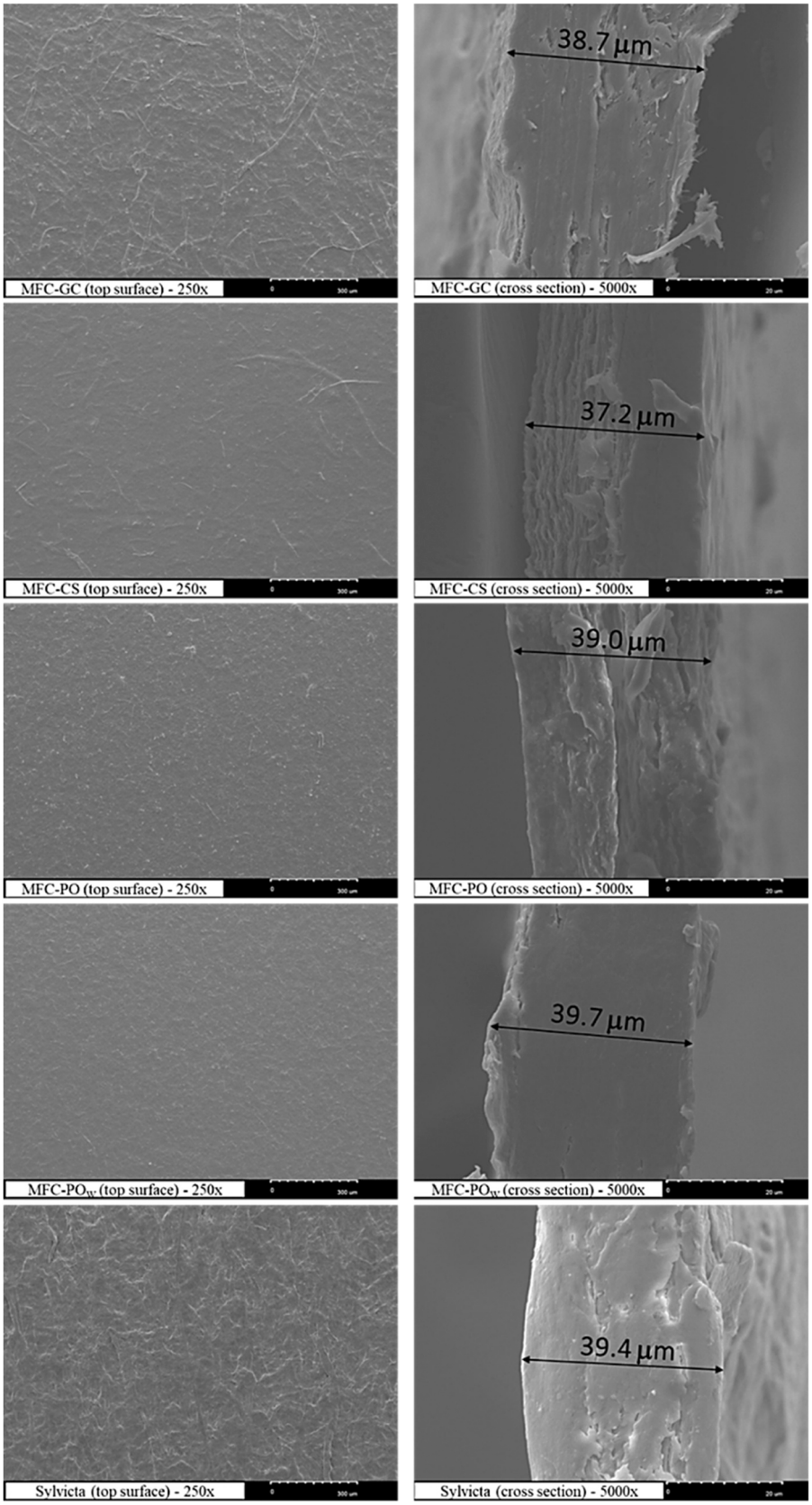


**Fig. 4.** SEM micrographs of the top surface (250 ×, on the left) and cross-section (5000 ×, on the right) of all films investigated in this work. The thickness of the films was also reported.

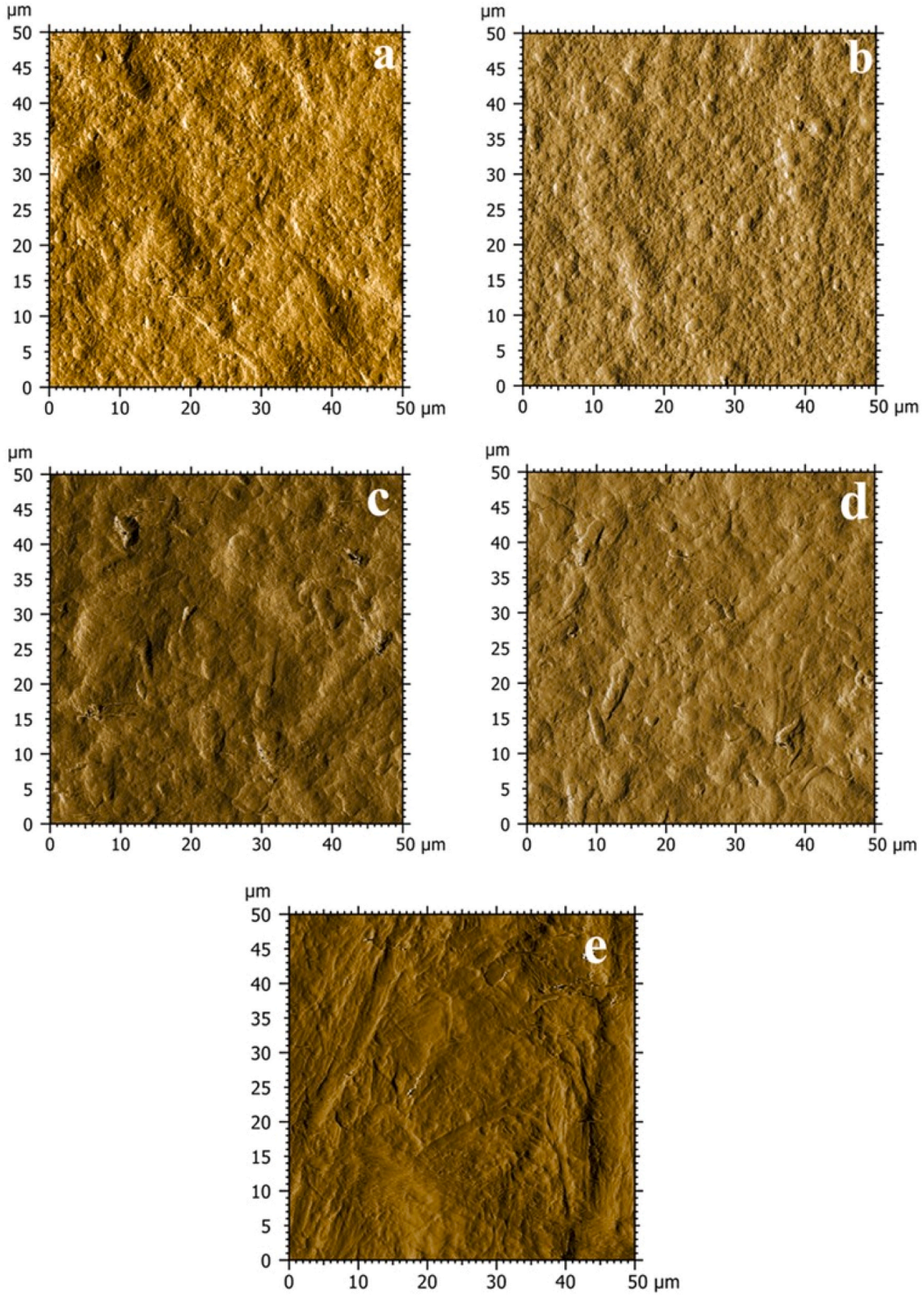


**Fig. 5.** AFM contact-resonance surface images (50 × 50 µm$^2$ in size) of MFC-GC (a), MFC-CS (b), MFC-PO (c), MFC-PO$_W$ (d), and Sylvicta® (e) samples.

matrix-dependent trend. Overall, the MFC films produced in this work showed comparable or superior performance to the commercial reference film Sylvicta®. In particular, the MFC-CS film exhibited a superior oxygen barrier at 50% RH, stronger UV-blocking properties, and higher tensile strength and elongation at break than Sylvicta®. The commercial film, however, was significantly more hydrophobic than the MFC films derived from biomasses. These results highlight the potential of MFC films derived from biomass to expand market opportunities in the bio-based food packaging sector. However, their moisture sensitivity (evidenced by a slight reduction in oxygen barrier performance at 50% RH and poor water vapor barrier properties) limits the use of pristine MFC films to niche applications such as dry pasta, rice, or tea bags.

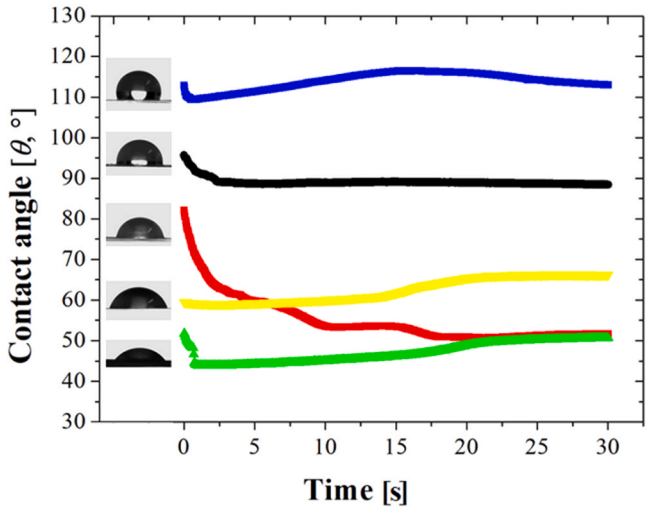


**Fig. 6.** Contact angle evolution (30 s time span) for the MFC-GC (black line), MFC-CS (red line), MFC-PO (green line), MFC-$PO_W$ (yellow line), and Sylvicta® (blue line) samples. The droplet image at $t_0$ (i.e., immediately after the droplet touched the sample surface) is shown on the left of each curve.

Alternatively, MFC dispersions can be employed in coating technologies, including the deposition of high oxygen barrier thin layers sandwiched between two protective films.

In conclusion, further studies are warranted to:

a) refine the formulation of the dispersion (e.g., by incorporating plasticizing agents to improve film extensibility and by optimizing the inclusion of hydrophobic components such as beeswax);
b) investigate additional biomasses for cellulose extraction and their influence on the final properties of both MFC dispersions and films;
c) evaluate the films' hygroscopicity as an indicator of their gas and vapor barrier performance;
d) assess the compostability of the resulting bio-packaging materials;
e) analyze the economic feasibility of HPH-based MFC production for potential scale-up;
f) conduct shelf-life studies across different food categories to compare the protective performance of MFC films with that of conventional petroleum-based plastics.

## Funding

This study was carried out within the Agritech National Research Center and received funding from the European Union Next-Generation EU (PIANO NAZIONALE DI RIPRESA E RESILIENZA (PNRR) – MISSIONE 4 COMPONENTE 2, INVESTIMENTO 1.4 – D.D. 1032 June 17, 2022, CN00000022). T. Bellesia's PhD contract was funded by the European Union – FSE, Research & Innovation 2014–2020 National Operative Program (DOT1315775–6 and 15-G-13883–1) and Fedrigoni Spa (FED_20220718_0030920126). D. Carullo's work was partially funded by the Early Career Development 2025 - Linea 8 del Piano di Sostgno alla Ricerca – PSR - Sottomisura A – Dote Ricerca RTT of the University of Milan.

## CRediT authorship contribution statement

**Tommaso Bellesia:** Writing – original draft, Investigation, Formal analysis, Data curation, Conceptualization. **Daniele Carullo:** Writing – review & editing, Supervision, Methodology, Investigation, Data curation, Conceptualization. **Andrea Fachin:** Writing – review & editing, Data curation. **Maral Soltanzadeh:** Writing – review & editing, Data curation. **Masoud Ghaani:** Writing – review & editing, Data curation. **Giorgio Innocenzo Ascrizzi:** Writing – original draft, Investigation, Formal analysis, Data curation. **Laura Piazza:** Writing – review & editing, Validation, Resources, Methodology, Data curation, Conceptualization. **Stefano Farris:** Writing – review & editing, Validation, Supervision, Resources, Project administration, Methodology, Investigation, Data curation, Conceptualization.

## Declaration of Competing Interest

The authors declare that they have no known competing financial interests or personal relationships that could have appeared to influence the work reported in this paper.

## Appendix A. Supporting information

Supplementary data associated with this article can be found in the online version at doi:10.1016/j.fpsl.2026.101728.

## Data availability

Data will be made available on request.

## References

Aguiló-Aguayo, I., Albaladejo, P., Gallur, M., Abadias, M., Ortiz, J., Vinas, I., & Lafarga, T. (2024). High added value products from agroindustrial residues: study on microfibrillated cellulose for food applications. *Waste and Biomass Valorization, 15*, 6723–6743. https://doi.org/10.1007/s12649-024-02605-1

Amoroso, L., De France, K. J., Milz, C. I., Siqueira, G., Zimmermann, T., & Nyström, G. (2022). Sustainable cellulose nanofiber films from carrot pomace as sprayable coatings for food packaging applications. *ACS Sustainable Chemistry & Engineering, 10*, 342–352. https://doi.org/10.1021/acssuschemeng.1c06345

Arafat, K. M. Y., Salem, K. S., Bera, S., Jameel, H., Lucia, L., & Pal, L. (2025). Surfactant-modified microfibrillated cellulose reinforcement of high-barrier sustainable packaging films. *Carbohydrate Polymers, 357*, Article 123471. https://doi.org/10.1016/j.carbpol.2025.123471

Araújo, D. J. C., Machado, A. V., & Vilarinho, M. C. L. G. (2019). Availability and suitability of agroindustrial residues as feedstock for cellulose-based materials: brazil case study. *Waste and Biomass Valorization, 10*, 2863–2878. https://doi.org/10.1007/s12649-018-0291-0

Bassani, A., Carullo, D., Rossi, F., Fiorentini, C., Garrido, G. D., Reklaitis, G. V. R., Bonadies, I., & Spigno, G. (2022). Modeling of a spray-drying process for the encapsulation of high-added value extracts from food by-products. *Computers and Chemical Engineering, 161*, Article 107772. https://doi.org/10.1016/j.compchemeng.2022.107772

Bellesia, T., Carullo, D., Fachin, A., Caneva, E., & Farris, S. (2024). A soft processing technology for the extraction of cellulose from plant residues and agri-food wastes. *Food Bioscience, 62*, Article 105141. https://doi.org/10.1016/j.fbio.2024.105141

Carullo, D., Abera, B. D., Casazza, A. A., Donsì, F., Perego, P., Ferrari, G., & Pataro, G. (2018). Effect of pulsed electric fields and high-pressure homogenization on the aqueous extraction of intracellular compounds from the microalgae Chlorella vulgaris. *Algal Research, 31*, 60–69. https://doi.org/10.1016/j.algal.2018.01.017

Carullo, D., Casson, A., Rovera, C., Ghaani, M., Bellesia, T., Guidetti, R., & Farris, S. (2023a). Testing a coated PE-based mono-material for food packaging applications: An in-depth performance comparison with conventional multi-layer configurations. *Food Packaging and Shelf Life, 39*, Article 101143. https://doi.org/10.1016/j.fpsl.2023.101143.

Carullo, D., Rovera, C., Bellesia, T., Büyüktas, D., Ghaani, M., Santo, N., Romano, D., & Farris, S. (2023b). Acid-derived bacterial cellulose nanocrystals as organic filler for the generation of high-oxygen barrier bio-nanocomposite coatings. *RSC Sustainable Food Technology, 1*, 941–950. https://doi.org/10.1039/D3FB00147D

Çavdaroğlu, E., Büyüktaş, D., Farris, S., & Yemenicioğlu, A. (2023). Novel edible films of pectins extracted from low-grade fruits and stalk wastes of sun-dried figs: Effects of pectin composition and molecular properties on film characteristics. *Food Hydrocolloids, 135*, Article 108136. https://doi.org/10.1016/j.foodhyd.2022.108136

Chandrasekar, C. M., Carullo, D., Saitta, F., Krishnamachari, H., Bellesia, T., Nespoli, L., Caneva, E., Baschieri, C., Signorelli, M., Barbiroli, A. G., Fessas, D., Farris, S., & Romano, D. (2024). Valorization of citrus peel industrial wastes for facile extraction of extractives, pectin, and cellulose nanocrystals through ultrasonication: An in-depth investigation. *Carbohydrate Polymers, 344*, Article 122539. https://doi.org/10.1016/j.carbpol.2024.122539

Cinar Ciftci, G., Larsson, P. A., Riazanova, A. V., Øvrebø, H. H., Wågberg, L., & Berglund, L. A. (2020). Tailoring of rheological properties and structural polydispersity effects in microfibrillated cellulose suspensions. *Cellulose, 27*, 9227–9241. https://doi.org/10.1007/s10570-020-03438-6

Coccaro, N., Ferrari, G., & Donsì, F. (2018). Understanding the break-up phenomena in an orifice-valve high pressure homogenizer using spherical bacterial cells (Lactococcus lactis) as a model disruption indicator. *Journal of Food Engineering, 236*, 60–71. https://doi.org/10.1016/j.jfoodeng.2018.05.011

Cozzolino, C. A., Campanella, G., Türe, H., Olsson, R. T., & Farris, S. (2016). Microfibrillated cellulose and borax as mechanical, O2-barrier, and surface-modulating agents of pullulan biocomposite coatings on BOPP. *Carbohydrate Polymers, 143*, 179–187. https://doi.org/10.1016/j.carbpol.2016.01.068

Dou, J., Vuorinen, T., Koivula, H., Forsman, N., Sipponen, M., & Hietala, S. (2021). Self-standing lignin-containing willow bark nanocellulose films for oxygen blocking and uv shielding. *ACS Applied Nano Matererials, 4*, 2921–2929. https://doi.org/10.1021/acsanm.1c00071

Dubey, P., Tripathi, G., Mir, S. S., & Yousuf, O. (2023). Current scenario and global perspectives of citrus fruit waste as a valuable resource for the development of food packaging film. *Trends in Food Science & Technology, 141*, Article 104190. https://doi.org/10.1016/j.tifs.2023.104190

Espinosa, E., Rincon, E., Morcillo-Martín, R., Rabasco-Vílchez, L., & Rodríguez, A. (2022). Orange peel waste biorefinery in multi-component cascade approach: Polyphenolic compounds and nanocellulose for food packaging. *Industrial Crops & Products, 187*, Article 115413. https://doi.org/10.1016/j.indcrop.2022.115413

Ezeorba, T. P. C., Okeke, E. S., Mayel, M. H., Nwuche, C. O., & Ezike, T. C. (2024). Recent advances in biotechnological valorization of agro-food wastes (AFW): Optimizing integrated approaches for sustainable biorefinery and circular bioeconomy. *Bioresource Technology Reports, 26*, Article 101823. https://doi.org/10.1016/j.biteb.2024.101823

Farris, S., Introzzi, L., Biagioni, P., Schiraldi, A., Holz, T., & Piergiovanni, L. (2011). Wetting of biopolymer coatings: contact angle kinetics and image analysis investigation. *Langmuir, 27*, 7563–7574. https://doi.org/10.1021/la2017006

Farris, S., Mora, L., Capretti, G., & Piergiovanni, L. (2012). Charge density quantification of polyelectrolyte polysaccharides by conductometric titration: An analytical chemistry experiment. *Journal of Chemical Education, 89*, 121–124. https://doi.org/10.1021/ed200261w

Farris, S. (2018). Engineering properties of packaging films. In In. M. W. Siddiqui, M. S. Rahman, & A. A. Wani (Eds.), *Innovative Packaging of Fruits and Vegetables: Strategies for Safety and Quality Maintenance* (pp. 211–226). Apple Academic Press Inc.

Fedrigoni. (2025). Meet Sylvicta. Retrieved from ⟨https://specialpapers.fedrigoni.com/sylvicta/⟩. Accessed November 25, 2025.

García, A., Gandini, A., Labidi, J., Belgacem, N., & Bras, J. (2016). Industrial and crop wastes: A new source for nanocellulose biorefinery. *Industrial Crops & Products, 93*, 26–38. https://doi.org/10.1016/j.indcrop.2016.06.004

Ghaani, M., Soltanzadeh, M., Carullo, D., & Farris, S. (2024). Development of a biopolymer-based anti-fog coating with sealing properties for applications in the food packaging sector. *Polymers, 16*, 1745. https://doi.org/10.3390/polym16121745

Ghasemlou, M., Barrow, C. J., & Adhikari, B. (2024). The future of bioplastics in food packaging: An industrial perspective. *Food Packaging and Shelf Life, 43*, Article 101279. https://doi.org/10.1016/j.fpsl.2024.101279

Hernández-Becerra, E., Osorio, M., Marín, D., Gañán, P., Pereira, M., Builes, D., & Castro, C. (2023). Isolation of cellulose microfibers and nanofibers by mechanical fibrillation in a water-free solvent. *Cellulose, 30*, 4905–4923. https://doi.org/10.1007/s10570-023-05162-3

Jiang, F., Nyström, G., & Budtova, T. (2025). Editorial to Special Issue: "Interactions between polysaccharides and water for advanced chemistry, structure and materials design. *Carbohydrate Polymers, 357*, Article 123492. https://doi.org/10.1016/j.carbpol.2025.123492

Jin, K., Tang, Y., Liu, J., Wang, J., & Ye, C. (2021). Nanofibrillated cellulose as coating agent for food packaging paper. *International Journal of Biological Macromolecules, 168*, 331–338. https://doi.org/10.1016/j.ijbiomac.2020.12.066

Khan, R., Jolly, R., Fatima, T., & Shakir, M. (2022). Extraction processes for deriving cellulose: A comprehensive review on green approaches. *Polymers Advanced Technologies, 33*, 2069–2090. https://doi.org/10.1002/pat.5678

Kim, H. J., Roy, S., & Rhim, J. W. (2021). Effects of various types of cellulose nanofibers on the physical properties of the CNF-based films. *Journal of Environmental Chemical Engineering, 9*, Article 106043. https://doi.org/10.1016/j.jece.2021.106043

Klangmuang, P., & Sothornvit, R. (2016). Combination of beeswax and nanoclay on barriers, sorption isotherm and mechanical properties of hydroxypropyl methylcellulose-based composite films. *LWT, 65*, 222–227. https://doi.org/10.1016/j.lwt.2015.08.003

Kumar, V., Nazari, Behzad, B., Bousfield, B., & Toivakka, M. (2016). Rheology of microfibrillated cellulose suspensions in pressure-driven flow. *Applied Rheology, 26*, 24–34. https://doi.org/10.3933/applrheol-26-43534

Lengowski, E. C., Bonfatti Júnior, E. A., Simon, L. C., Bolzon de Muniz, G. I., de Andrade, A. S., Leite, A. N., & de Miranda Leite, E. L. S. (2023). Nanocellulose coating on kraft paper. *Coatings, 13*, 1705. https://doi.org/10.3390/coatings13101705

Li, P., Zhou, M., Jian, B., Lei, H., Liu, R., Zhou, X., Li, X., Wang, Y., & Zhou, B. (2023). Paper material coated with soybean residue nanocellulose waterproof agent and its application in food packaging. *Industrial Crops & Products, 199*, Article 116749. https://doi.org/10.1016/j.indcrop.2023.116749

Liu, X., Jiang, Y., Wang, L., Song, X., Qin, C., & Wang, S. (2020). Tuning of size and properties of cellulose nanofibers isolated from sugarcane bagasse by endoglucanase-assisted mechanical grinding. *Industrial Crops & Products, 146*, Article 112201. https://doi.org/10.1016/j.indcrop.2020.112201

Luo, Y., Wu, Y., Wang, Y., & Yu, L. (2021). Active and robust composite films based on gelatin and gallic acid integrated with microfibrillated cellulose. *Foods, 10*, 2831. https://doi.org/10.3390/foods10112831

Mapelli, F., Carullo, D., Farris, S., Ferrante, A., Bacenetti, J., Ventura, V., Frisio, D., & Borin, S. (2022). Food waste-derived biomaterials enriched by biostimulant agents for sustainable horticultural practices: A possible circular solution. *Frontiers in Sustainability, 2*, Article 928970. https://doi.org/10.3389/frsus.2022.928970

Mayrhofer, A., Kopacic, S., & Bauer, W. (2023). Extensive characterization of alginate, chitosan and microfibrillated cellulose cast films to assess their suitability as barrier coating for paper and board. *Polymers, 15*, 3336. https://doi.org/10.3390/polym15163336

Mengozzi, A., Carullo, D., Bot, F., Farris, S., & Chiavaro, E. (2024). Functional properties of food packaging solutions alternative to conventional multilayer systems. *Journal of Food Science & Technology*. https://doi.org/10.1007/s13197-024-06038-5

Mujtaba, M., Lipponen, J., Ojanen, M., Puttonen, S., & Vaittinen, H. (2022). Trends and challenges in the development of bio-based barrier coating materials for paper/cardboard food packaging; a review. *Science of the Total Environment, 851*, Article 158328. https://doi.org/10.1016/j.scitotenv.2022.158328

Orqueda, M. E., Méndez, D. A., Martínez-Abad, A., Zampini, C., Torres, S., Isla, M. I., Lopez-Rubio, A., & Fabra, M. J. (2022). Feasibility of active biobased films produced using red chilto wastes to improve the protection of fresh salmon fillets via a circular economy approach. *Food Hydrocolloids, 133*, Article 107888. https://doi.org/10.1016/j.foodhyd.2022.107888

Ortiz, C. M., Salgado, P. R., Dufresne, A., & Mauri, A. N. (2018). Microfibrillated cellulose addition improved the physicochemical and bioactive properties of biodegradable films based on soy protein and clove essential oil. *Food Hydrocolloids, 79*, 416–427. https://doi.org/10.1016/j.foodhyd.2018.01.011

Padhi, S., Singh, A., & Routray, W. (2023). Nanocellulose from agro-waste: a comprehensive review of extraction methods and applications. *Reviews in Environmental Science and Bio/Technology, 22*, 1–27. https://doi.org/10.1007/s11157-023-09643-6

Pirozzi, A., Capuano, R., Avolio, R., Gentile, G., Ferrari, G., & Donsì, F. (2021). O/W Pickering emulsions stabilized with cellulose nanofibrils produced through different mechanical treatments. *Foods, 10*, 1886. https://doi.org/10.3390/foods10081886

Pirozzi, A., Olivieri, F., Castaldo, R., Gentile, G., & Donsì, F. (2023). Cellulose isolation from tomato pomace: part ii—integrating high-pressure homogenization in a cascade hydrolysis process for the recovery of nanostructured cellulose and bioactive molecules. *Foods, 12*, 3221. https://doi.org/10.3390/foods12173221

Qi, Y., Zhang, H., Xu, D., He, Z., Pan, X., Gui, S., Dai, X., Fan, J., Dong, X., & Li, Y. (2020). Screening of nanocellulose from different biomass resources and its integration for hydrophobic transparent nanopaper. *Molecules, 25*, 227. https://doi.org/10.3390/molecules25010227

Ramos, M., Laveriano, E., San Sebastian, L., Perez, M., Jimenez, A., Lamuela-Raventos, R. M., Garrigos, M. C., & Vallverdú-Queralt, A. (2023). Rice straw as a valuable source of cellulose and polyphenols: Applications in the food industry. *Trends in Food Science & Technology, 131*, 14–27. https://doi.org/10.1016/j.tifs.2022.11.020

Rantanen, J., Dimic-Misic, K., Pirttiniemi, J., Kuosmanen, P., & Maloney, T. C. (2015). Forming and dewatering of a microfibrillated cellulose composite paper. *BioResources, 10*, 3492–3506. https://doi.org/10.15376/biores.10.2.3492-3506

Romruen, O., Karbowiak, T., Tongdeesoontorn, W., Shiekh, K. A., & Rawdkuen, S. (2022). Extraction and characterization of cellulose from agricultural by-products of chiang rai province, Thailand. *Polymers, 14*, 1830. https://doi.org/10.3390/polym14091830

Rostamabadi, H., Demirkesen, I., Colussi, R., Roy, S., Tabassum, N., de Oliveira Filho, J. G., Bist, Y., Kumar, Y., Nowacka, M., Galus, M., & Falsafi, S. R. (2024). Recent trends in the application of films and coatings based on starch, cellulose, chitin, chitosan, xanthan, gellan, pullulan, Arabic gum, alginate, pectin, and carrageenan in food packaging. *Food Frontiers, 5*, 350–391. https://doi.org/10.1002/fft2.342

Rovera, C., Türe, H., Hedenqvist, M. S., & Farris, S. (2020). Water vapor barrier properties of wheat gluten/silica hybrid coatings on paperboard for food packaging applications. *Food Packaging and Shelf Life, 26*, Article 100561. https://doi.org/10.1016/j.fpsl.2020.100561

Rovera, C., Carullo, D., Bellesia, T., Büyüktas, D., Ghaani, M., Caneva, E., & Farris, S. (2023). Extraction of high-quality grade cellulose and cellulose nanocrystals from different lignocellulosic agri-food wastes. *Frontiers in Sustainable Food Systems, 6*, Article 1087867. https://doi.org/10.3389/fsufs.2022.1087867

Sabater, C., Villamiel, M., & Montilla, A. (2022). Integral use of pectin-rich by-products in a biorefinery context: A holistic approach. *Food Hydrocolloids, 128*, Article 107564. https://doi.org/10.1016/j.foodhyd.2022.107564

Salas, C., Nypelö, T., Rodriguez-Abreu, C., Carrillo, C., & Rojas, O. J. (2014). Nanocellulose properties and applications in colloids and interfaces. *Current Opinion in Colloid & Interface Science, 19*, 383–396. https://doi.org/10.1016/j.cocis.2014.10.003

Samsalee, N., Meerasri, J., & Sothornvit, R. (2023). Rice husk nanocellulose: Extraction by high-pressure homogenization, chemical treatments and characterization. *Carbohydrate Polymer Technologies and Applications, 6*, Article 100353. https://doi.org/10.1016/j.carpta.2023.100353

Sayanjali, S., Lu, Y., & Howell, K. (2024). Extraction and characterization of cellulose from broccoli stems as a new biopolymer source for producing carboxymethyl cellulose films. *International Journal of Food Science, 2024*, Article 7661288. https://doi.org/10.1155/2024/7661288

Schiessl, S., Kucukpinar, E., Rivollier, N., Langowski, H.-C., & Eisner, P. A. (2023). Comparative study on the roll-to-roll processing of a silicate–polyvinyl alcohol composite barrier lacquer using slot-die and reverse gravure coating techniques. *Polymers, 15*, 2761. https://doi.org/10.3390/polym15132761

Shorey, R., & Mekonnen, T. H. (2022). Sustainable paper coating with enhanced barrier properties based on esterified lignin and PBAT blend. *International Journal of Biological Macromolecules, 209*, 472–484. https://doi.org/10.1016/j.ijbiomac.2022.04.037

Spence, K. L., Venditti, R. A., Rojas, O. J., Habibi, Y., & Pawlak, J. J. (2010). The effect of chemical composition on microfibrillar cellulose films from wood pulps: water interactions and physical properties for packaging applications. *Cellulose, 17*, 835–848. https://doi.org/10.1007/s10570-010-9424-8

Suksri, C., & Aht-Ong, D. (2022). Preparation of cellulose nanofibers from cassava pulp residue by mechanical defibrillation. *Journal of Physics: Conference Series, 2175*, Article 012039. https://doi.org/10.1088/1742-6596/2175/1/012039

Svärd, A., Moriana, R., Brännvall, E., & Edlund, E. (2019). Rapeseed straw biorefinery process. *ACS Sustainable Chemistry & Engineering, 7*, 790–801. https://doi.org/10.1021/acssuschemeng.8b04420

Thomas, A. P., Kasa, V. P., Dubey, B. K., Sen, R., & Sarmah, A. K. (2023). Synthesis and commercialization of bioplastics: Organic waste as a sustainable feedstock. *Science of the Total Environment, 904*, Article 167243. https://doi.org/10.1016/j.scitotenv.2023.167243

Thongsomboon, W., Baimark, Y., & Srihanam, P. (2023). Valorization of cellulose-based materials from agricultural waste: comparison between sugarcane bagasse and rice straw. *Polymers, 15*, 3190. https://doi.org/10.3390/polym15153190

Tibolla, H., Pelissari, F. M., Martins, J. T., Vicente, A. A., & Menegalli, F. C. (2018). Cellulose nanofibers produced from banana peel by chemical and mechanical treatments: Characterization and cytotoxicity assessment. *Food Hydrocolloids, 75*, 192–201. https://doi.org/10.1016/j.foodhyd.2017.08.027

Urena, M., Carullo, D., Phùng, T. T. T., Fournier, P., Farris, S., Lagorce, A., & Karbowiak, T. (2024). Effect of polymer structure on the functional properties of alginate for film or coating applications. *Food Hydrocolloids, 149*, Article 109557. https://doi.org/10.1016/j.foodhyd.2023.109557

Wang, F.-j, Wang, L.-q, Zhang, X.-c, Ma, S.-f, & Zhao, Z.-c (2022). Study on the barrier properties and antibacterial properties of cellulose-based multilayer coated paperboard used for fast food packaging. *Food Bioscience, 46*, Article 101398. https://doi.org/10.1016/j.fbio.2021.101398

Wang, Y., Wang, Z., Lin, Y., Qin, Y., He, R., Wang, M., Sun, Q., & Peng, Y. (2024). Nanocellulose from agro-industrial wastes: A review on sources, production, applications, and current challenges. *Food Research International, 192*, Article 114741. https://doi.org/10.1016/j.foodres.2024.114741

Wei, L., Bian, H., Agarwal, U. P., Sabo, R. C., Matuana, L. M., & Stark, N. M. (2023). Correlation between morphology and performance of cellulose nanofibril-based films. *Current Research in Greening and Sustainable Chemistry, 6*, Article 100363. https://doi.org/10.1016/j.crgsc.2023.100363

Wu, C., McClements, D. J., He, M., Zheng, L., Tian, T., Teng, F., & Li, Y. (2021). Preparation and characterization of okara nanocellulose fabricated using sonication or high-pressure homogenization treatments. *Carbohydrate Polymers, 255*, Article 117364. https://doi.org/10.1016/j.carbpol.2020.117364

Yao, C., Li, F., Chen, T.-Y., & Tang, Y. (2023). Green preparation of cellulose nanofibers via high-pressure homogenization and their film-forming properties. *Industrial Crops and Products, 206*, Article 117575. https://doi.org/10.1016/j.indcrop.2023.117575

Yu, W., Luo, L., Yi, Y., Xing, C., Yang, Y., Tang, Z., Guo, X., Tan, Z., & Tam, K. C. (2024). Active food packaging composite films from bast fibers-derived cellulose nanofibrils. *ACS Sustainable Chemistry & Engineering, 12*, 9511–9521. https://doi.org/10.1021/acssuschemeng.4c03117

Zhang, W., Zhang, X., Ren, S., Dong, L., Ai, Y., Lei, T., & Wu, Q. (2023). Lignin containing cellulose nanofiber based nanopapers with ultrahigh optical transmittance and haze. *Cellulose, 30*, 5967–5985. https://doi.org/10.1007/s10570-023-05244-2